Journal of Inorganic and Organometallic Polymers and Materials (2020) 30:477–485
https://doi.org/10.1007/s10904-019-01206-z

Syntheses, Crystal Structures and Theoretical Calculations of Two Nickel, Zinc Coordination Polymers with 4-Nitrophthalic Acid and Bis(imidazol) Ligands

Xiu-Mei Li[1] · Zhi-Tao Wang[1,2] · Valentin Valtchev[2] · Qian-Rong Fang[2] · Ya-Ru Pan[1]

Received: 17 March 2019 / Accepted: 23 May 2019 / Published online: 3 June 2019

Abstract
Two new complexes $[Ni(4\text{-nph})(bix)(H_2O)]_n$ **(1)** and $[Zn(4\text{-nph})(mbix)]_n{\cdot}nH_2O$ **(2)** ($4\text{-}H_2nph$ = 4-nitrophthalic acid, bix = 1,4-bis(imidazol-1-yl)-benzene, mbix = 1,3-bis(imidazol-1-yl)-benzene) have been hydrothermally synthesized and structurally characterized by elemental analysis, IR spectroscopy, TG, fluorescence spectroscopy, single-crystal and powder X-ray diffraction. Complex **1** exhibits two dimensional (2D) network structure contain 42-number ring and complex **2** shows one-dimensional ribbon, which were further extended into three-dimensional supramolecular structure through hydrogen bonds and π–π stacking interactions. Moreover, we analyzed the natural bond orbital using the PBE0/LANL2DZ method in the Gaussian 03 program of complexes **1** and **2**. The calculation results indicated the obvious covalent interactions between the coordinated atoms and the Ni^{II}, Zn^{II} ion respectively.

Keywords Hydrothermal synthesis · Crystal structure · Ni(II) complex · Zn(II) complex · Natural bond orbital

1 Introduction

The crystal engineering of metal coordination polymers (MCPs) is one of the most rapidly developing areas of chemical science owing to their diversity of type and physical–chemical properties [1–4]. Obviously, it is the important responsibility for chemists to rationally design and synthesize more MCPs with diverse structures. It is well known that the assembly processes and structures of MCPs are influenced by many factors, such as the coordination preferences of metal ions [5, 6], the conformation of bridging ligands [7], solvent systems [8], counteranion [9] and pH value of the solution [10] which can also affect the nature of coordination networks and the framework formation.

In recent years, the direct use of two types of organic ligands has been found to be an effective method for the synthesis of MCPs. Aromatic carboxylate ligands are frequently chosen to construct various dimensions of MCPs because of their rich coordination modes, including monodentate, bridging and chelating. For example, benzoic acid, 1,3-benzenedicarboxylate, 1,4-benzenedicarboxylate, 1,2-benzenedicarboxylate, and 1,2,4,5-benzene tetracarboxylate [11–14] are well used in the construction of MCPs due to their structural rigidity, chemical stability and appropriate connectivity. Besides the carboxylate linkers, bis(imidazole) bridging ligands with different length and flexibly, for example, 1,3-bis(imidazol-1-ylmethyl)-benzene, 1,4-bis(imidazol-1-ylmethyl)-benzene, 1,4-bis(1H-benzimidazolyl)butane are frequently used in the assembly process of MCPs as bridging linker [15–18].

In view of these factors, we herein report the synthesis and characteristics of two new complexes containing 4-nitrophthalic acid and 1,4-bis(imidazol-1-ylmethyl)- benzene/1,3-bis(imidazol-1-ylmethyl)-benzene namely, $[Ni(4\text{-nph})(bix)(H_2O)]_n$ **(1)** and $[Zn(4\text{-nph})(mbix)]_n{\cdot}nH_2O$ **(2)**.

✉ Valentin Valtchev
laowa2017@163.com

[1] Faculty of Chemistry, Tonghua Normal University, Tonghua 134002, China

[2] State Key Laboratory of Inorganic Synthesis and Preparative Chemistry, Jilin University, Changchun 130012, China

2 Experimental

2.1 General Procedures

All reagents were purchased commercially and used without further purification. Elemental analyses (C, H and N) were measured on a Vario EL(III) Elemental Analyzer. IR spectrum was recorded in the range of 4000–400 cm^{-1} on an Nicolet 6700 Spectrophotometer using a KBr pellet. Powder X-ray diffraction (PXRD) patterns were collected in the 2θ range of 5°–50° with a scan speed of 0.1°/s on a Bruker D8 Advance instrument using a CuKα radiation ($\lambda = 1.54056$ Å) at room temperature. The TG studies were performed on a Perkin-Elmer TGA7 analyzer. The fluorescent studies were carried out on a computer-controlled JY Fluoro-Max-3 spectrometer at room temperature.

2.2 Synthesis

2.2.1 $[Ni(4\text{-nph})(bix)(H_2O)]_n$ (1)

A mixture of $Ni(OAc)_2{\cdot}4H_2O$ (0.2 mmol, 0.0498 g), 4-H_2nph (0.2 mmol, 0.0418 g) and bix (0.2 mmol, 0.048 g) was dissolved in 15 mL H_2O. The final mixture was placed in a Parr Teflon-lined stainless-steel vessel (25 mL) under autogenous pressure and heated at 140 °C for 5 days. The crystals of parallelogram were obtained. The yield of the reaction was ca. 29% based on Ni. Calcd. for $C_{22}H_{17}N_5NiO_8$: C, 49.11; H, 3.18; N, 13.02%. Found: C, 48.91; H, 2.98; N, 12.82%. IR (KBr, cm^{-1}): 3589(w), 3152(w), 1638(m), 1627(s), 1561(s), 1517(m), 1483(w), 1432(m), 1404(m), 1377(w), 1347(m), 1243(m), 1202(w), 1104(m), 1088(w), 1065(w), 1028(w), 944(m), 846(m), 754(w), 737(w), 661(m), 622(w), 600(w), 531(w), 481(w).

2.2.2 $[Zn(4\text{-nph})(mbix)]_n{\cdot}nH_2O$ (2)

A mixture of $Zn(OAc)_2{\cdot}2H_2O$ (0.2 mmol, 0.044 g), 4-H_2nph (0.2 mmol, 0.0418 g) and bix (0.2 mmol, 0.048 g) was dissolved in 15 mL H_2O. The final mixture was placed in a Parr Teflon-lined stainless-steel vessel (25 mL) under autogenous pressure and heated at 120 °C for 7 days. The crystals of block were obtained. The yield of the reaction was ca. 26% based on Zn. Calcd. for $C_{22}H_{19}N_5O_7Zn$: C, 49.78; H, 3.61; N, 13.19%. Found: C, 49.01; H, 3.08; N, 12.62%. IR (KBr, cm^{-1}): 3536(w), 3424(w), 3135(w), 1625(s), 1581(w), 1520(s), 1481(w), 1392(m), 1348(m), 1245(w), 1160(w), 1108(s), 1066(m), 1027(w), 956(m), 925(w), 832(s), 780(w), 766(m), 656(m), 610(w), 460(w), 440(w).

2.3 X-Ray Crystallography

Single-crystal X-ray diffraction data for **1** and **2** were recorded on a Bruker D8 QUEST CMOS diffractometer with graphite-monochromated Mo Kα radiation ($\lambda = 0.71073$ Å) at 293 K. The structure was solved with the direct method of SHELXS-97 and refined with full-matrix least-squares techniques using the SHELXL-97 program [19, 20]. The non-hydrogen atoms of the complexes were refined with anisotropic temperature parameters. The hydrogen atoms attached to carbons were generated geometrically. Crystallographic parameters and the data collection statistics for structure **1** and **2** are given in Table 1. Selected bond lengths and bond angles are listed in Table 2. Further crystallographic parameters have been deposited with the Cambridge Crystallographic Data Centre (no. 1880194 **(1)**, 1903653 **(2)**; deposit@ccdc.cam.ac.uk or http://www.ccdc.cam.ac.uk/data_request/cif).

3 Results and Discussion

3.1 Structure Description of the Complexes 1 and 2

Compound **1** crystallizes in monoclinic crystal system with *P21/m* space group and features a two dimensional (2D) network structure. The coordination environment of Ni(II) in **1** is shown in Fig. 1. There are one crystallographically unique Ni(II) centers, one 4-nph ligand,

Table 1 Crystallographic parameters and summary of data collection for **1** and **2**

Parameter	Complex **1**	Complex **2**
Empirical formula	$C_{22}H_{17}N_5NiO_8$	$C_{22}H_{19}N_5O_7Zn$
Fw (g/mol)	538.12	530.66
Crystal system	Monoclinic	Triclinic
Space group	P2(1)/m	P − 1
a [Å]	7.3258 (6)	10.5969 (5)
b [Å]	14.1892 (10)	11.0384 (6)
c [Å]	10.7954 (8)	11.5575 (6)
α [°]	90.00	68.7340 (10)
β [°]	99.932 (2))	68.1400 (10)
γ [°]	90.00	84.9570 (10)
Volume [$Å^3$]	1105.33 (14)	1167.53 (10)
Z	2	2
D_c (g/cm^3)	1.617	1.509
GOF	1.024	1.074
Reflns collected/unique	7299/2042	4293/2507
R_{int}	0.0586	0.0285
*R*1 [I > 2σ(I)]	0.0636	0.0400

Table 2 Selected bond lengths (Å) and bond angles (°) for **1** and **2**

1			
Bond	*d* (Å)	Bond	*d* (Å)
Ni(1)–O(1)	2.012 (5)	Ni(1)–O(3A)	2.168 (3)
Ni(1)–O(3B)	2.168 (3)	Ni(1)–O(6)	2.079 (6)
Ni(1)–N(1)	2.037 (4)	Ni(1)–N(1C)	2.037 (4)
Angle	ω (°)	Angle	ω (°)
O(1)–Ni(1)–N(1)	98.46 (16)	O(1)–Ni(1)–N(1C)	98.46 (16)
N(1)–Ni(1)–N(1C)	101.3 (2)	O(1)–Ni(1)–O(6)	168.0 (2)
N(1)–Ni(1)–O(6)	89.08 (17)	N(1C)–Ni(1)–O(6)	89.08 (17)
O(1)–Ni(1)–O(3A)	86.48 (15)	N(1)–Ni(1)–O(3A)	98.43 (15)
O(6)–Ni(1)–O(3A)	83.22 (18)	O(1)–Ni(1)–O(3B)	86.48 (15)
N(1)–Ni(1)–O(3B)	158.69 (15)	O(6)–Ni(1)–O(3B)	83.22 (18)
2			
Bond	*d* (Å)	Bond	*d* (Å)
Zn(1)–O(1)	1.962 (3)	Zn(1)–O(3A)	1.955 (2)
Zn(1)–N(1)	1.986 (3)	Zn(1)–N(4B)	2.013 (3)
Angle	ω (°)	Angle	ω (°)
O(3A)–Zn(1)–O(1)	107.48 (12)	O(3A)–Zn(1)–N(1)	114.03 (12)
O(1)–Zn(1)–N(1)	113.48 (12)	O(3A)–Zn(1)–N(4B)	107.77 (12)
O(1)–Zn(1)–N(4B)	101.32 (12)	N(1)–Zn(1)–N(4B)	111.85 (13)

Symmetry codes: **1**: A: x − 1, y, z; B: x − 1, − y + 1/2, z; C: x, − y + 1/2, z

2: A:2 − x, 1 − y, 1 − z; B: 2 − x, 1 − y, − z

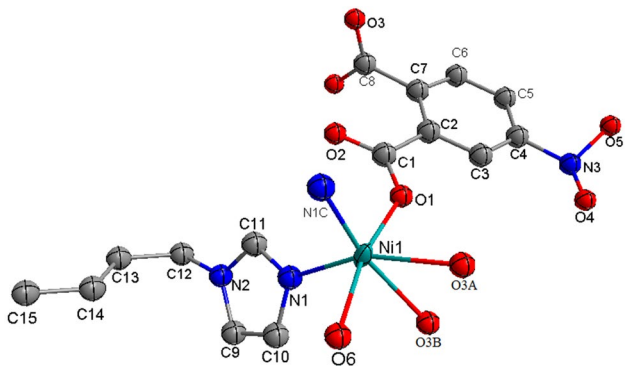

Fig. 1 The coordination environment of the Ni(II) center in **1**. Symmetry codes: (A) x − 1, y, z; (B) x − 1, − y + 1/2, z; (C) x, − y + 1/2, z

one bix ligand and one coordinated water molecule in the asymmetric unit. Ni(1) displays the six-coordinated octahedral geometry with different bond lengths and bond angles coordinated by three carboxylic oxygen atoms from two different 4-nph^{2-} ligands, two nitrogen atoms from two different bix ligands and one coordinated water molecule. The Ni–O bond distances fall in the 2.012(5)–.168(3) Å range, and the Ni–N bond distance is 2.037(4) Å, which are all similar to those for other previously reported Ni(II) complexes [21].

It is interesting to note that one carboxylate of 4-nph^{2-} anion coordinates with one Ni(II) atom in a chelating mode, while another carboxylate bridges one Ni(II) atom in a bridging mode. Notably, the bix ligand adopts a *anti*-conformation bridging mode with a dihedral angle between the two imidazole rings of 0°, based on this, four Ni(II) ions are linked by two bix and two 4-nph ligands to yield two dimensional network structure contain 42-number ring (Fig. 2).

Further investigation of the crystal packing of complex **1** suggests that there are persistent *π*–*π* interactions in complex **1** between imidazole rings of bix ligands (Fig. 3). The centroid-to-centroid distance between adjacent ring is 3.962(4) Å for N1C10C9N2C11 and N1'C10'C9'N2'C11' (Symmetry codes: 2 − *x*, − *y*, *z*) imidazole rings. The perpendicular distance is 3.606(3) Å for N1C10C9N2C11 and N1'C10'C9'N2'C11' (Symmetry codes: 2 − *x*, − *y*, *z*) imidazole rings. Moreover, there are C–H···O hydrogen bonding interactions in oxygen atoms and carbon atoms in complex **1** (Table 3). Therefore, through *π*–*π* stacking and hydrogen bonding interactions, complex **1** is further extended into a three-dimensional supramolecular framework.

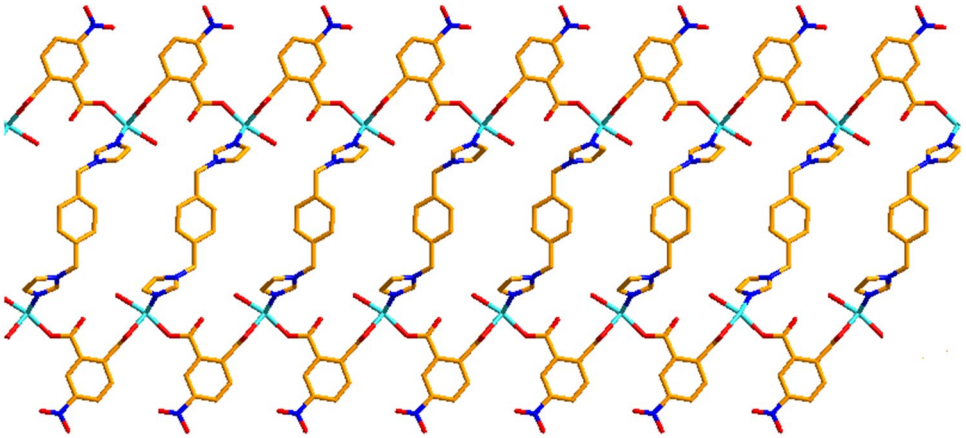

Fig. 2 View of the 2D network structure contain 42-number ring of complex **1**

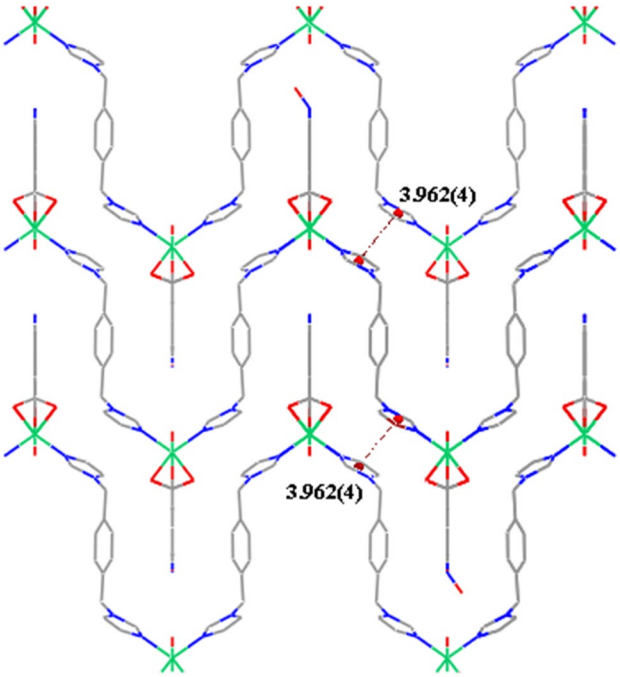

Fig. 3 View of the π–π interactions of complex **1**

Table 3 Hydrogen bonds for complexes **1** and **2**

D–H···A	d (D–H)	d (H···A)	d (D···A)	∠DHA
1				
C(3)–H(3)···O(1)	0.78 (10)	2.38 (10)	2.675 (9)	104 (8)
C(3)–H(3)···O(4)	0.78 (10)	2.45 (11)	2.720 (11)	102 (8)
C(5)–H(5)···O(5)$^{\#1}$	0.99 (13)	2.38 (11)	2.746 (15)	101 (7)
C(6)–H(6)···O(4)$^{\#2}$	1.06 (8)	2.54 (8)	3.477 (11)	147 (6)
C(11)–H(11)···O(2)	1.00 (6)	2.52 (5)	3.153 (7)	121 (4)
C(11)–H(11)···O(5)$^{\#3}$	1.00 (6)	2.49 (5)	3.275 (13)	135 (4)
C(12)–H(12A)···O(1)$^{\#4}$	0.96	2.54	3.483(7)	168
2				
OW(1)–HW(1)···O(3)$^{\#1}$	0.81	2.28	3.074 (5)	168
OW(1)–HW(2)···O(2)$^{\#2}$	0.83	2.20	2.815 (5)	130
C(10)–H(10A)···OW(1)$^{\#3}$	0.93	2.47	3.268 (6)	144
C(11)–H(11A)···O(2)	0.93	2.38	3.086 (5)	133
C(19)–H(19B)···O(4)$^{\#2}$	1.12(6)	2.49(6)	3.471 (6)	146 (4)
C(20)–H(20A)···OW(1)$^{\#4}$	1.04(5)	2.18(5)	3.161 (5)	156 (5)
C(22)–H(22A)···O(4)$^{\#2}$	0.93	2.42	3.198 (6)	141

Symmetry codes: **1**: #1: x, $1/2-y$, z; #2: $1+x$, y, z; #3:x, y, $-1+z$; #4: $-x$, $-1/2+y$, $-z$

2: #1: $-1+x$, y, z; #2: $1-x$, $1-y$, $1-z$; #3:$1+x$, $-1+y$, z; #4: $1+x$, y, z

Single crystal X-ray analysis revealed that the asymmetric unit of complex **2** is composed of one crystallographically Zn(II) ion, one unique mbix ligands, one unique 4-nph ligand and one crystal water molecule (Fig. 4). Each Zn(II) ion is four-coordinated by two nitrogen atoms (N1 and N4B) from two different mbix ligands, and two oxygen atoms from two different 4-nph ligands (O1, O3A) in a distorted tetrahedral coordination sphere. The Zn–O bond distances range from 1.955(2) to 1.962(3) Å, and the Zn-N distances vary from 1.986(3) to 2.013(3) Å. The N(O)–Zn–O(N) angles fall in the 101.32(12)°–14.03(12)° range.

In the complex **2**, the mbix ligands take *cis*-conformation bridging mode with a dihedral angle between the two imidazole rings of 47.82°, the 4-nph ligand coordinates to Zn(II) ions in a monodentate bridging fashion. As depicted in Fig. 5, Zn(II) ions are bridged by 4-nph and mbix ligands to give crystallographically dimers, with Zn1···Zn1A distance of 5.324, 7.576 Å respectively, and exhibits one-dimensional ribbon structure. Further analysis of the crystal packing revealed that there are hydrogen bonds between carbon atoms, crystal water molecule and carboxylic oxygen atoms (Table 3), undoubtedly they play an important role in the stabilization of complex **2**. In addition, between two adjacent imidazole rings of mbix ligand, two adjacent benzene rings of 4-nph ligand, imidazole ring of mbix ligand and benzene ring of 4-nph ligand, the shortest separation of 3.802(2) Å

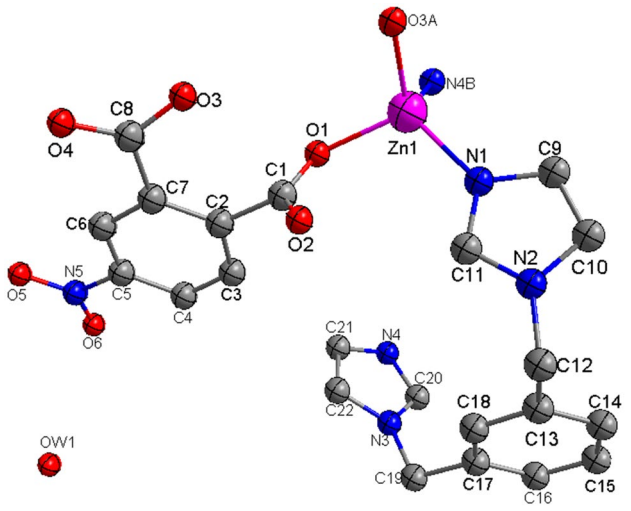

Fig. 4 The coordination environment of the Zn(II) center in **2**. Symmetry codes: (A) 2 − x, 1 − y, 1 − z; (B) 2 − x, 1 − y, − z

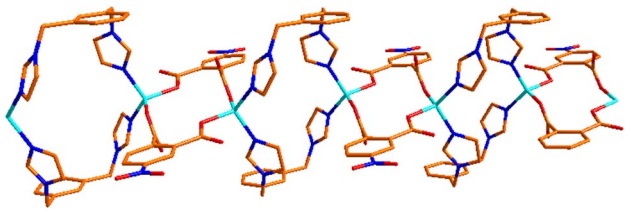

Fig. 5 View of the 1D ribbon of complex **2**

indicates that π–π stacking interactions (Table 4) further stabilize this one-dimensional structure, which are further extended into a three dimensional supramolecular framework (Fig. 6) through hydrogen bonds and π–π interactions. The type of π–π stacking may be of interest to the design of advanced materials.

3.2 Spectral Characterization and Thermal Properties of Complexes 1 and 2

IR spectrum of **1** shows a broad absorption band at 3589 cm^{-1}, corresponding to the H···O stretching of coordinated water molecules in the complex. Asymmetric and symmetric COO^- stretching modes of the lattice 4-nph^{2-} anion were evidenced by very strong, slightly broadened bands at 1627, 1561 and 1404 cm^{-1} [22], which is consistent with the results of X-ray analysis.

IR spectrum of **2** shows a broad absorption band at 3536 cm^{-1}, corresponding to the H···O stretching of coordinated water molecules in the complex. Asymmetric and symmetric COO^- stretching modes of the lattice 4-nph^{2-} anion were evidenced by very strong, slightly broadened bands at 1625, 1581 and 1392 cm^{-1} [19], which is consistent with the results of X-ray analysis.

To determine the thermal stability of complex **1** and **2**, their thermal behavior were investigated under nitrogen atmosphere by thermogrametric analysis (TG). As depicted in Fig. 7, the TG curve of **1** show that the complex **1** is stable up to 250 °C, and then decompose upon further heating. The thermal behavior of complex **2** is stable up to 320 °C, and then decompose upon further heating.

3.3 Powder X-Ray Diffraction (PXRD)

To confirm the phase purity of complexes **1** and **2**, powder X-ray diffraction (PXRD) patterns were recorded for **1** and **2**, and they were comparable to the corresponding simulated patterns calculated from the single-crystal diffraction data (Fig. 8), indicating a pure phase of bulky sample.

3.4 Photoluminescent Properties of Complexes 1 and 2

Taking into account the excellent luminescent properties of the imidazole species and metal ions compounds, the luminescence behaviors of complexes with nitrogen and carboxylate donor ligands have been a subject of immense current research [23]. MCPs have been reported to exhibit high thermal stability and the ability to tune the emission intensity of the free organic ligands after coordination with metals [24]. So, the solid state luminescence spectra of **1**, **2** (Fig. 9) and free ligands 4-H_2nph, bix, mbix were investigated at room temperature. The free 4-H_2nph, bix, and mbix ligand exhibits the emission at 440 nm, 508 nm,

Table 4 Parameters between the planes in **2**

Plane	Distance between ring centroids (Å)	Dihedral angle (°)	Perpendicular distance of Plane(I) on ring J (Å)	Perpendicular distance of Plane(J) on ring I (Å)
Plane(1) –> Plane(1)[2756]	3.925 (2)	0	3.6432 (17)	3.6433 (17)
Plane(4) –> Plane(4)[2666]	3.905 (2)	0	− 3.8332 (16)	− 3.8331 (16)
Plane(4) –> Plane(5)[1565]	3.802 (2)	6.2(2)	− 3.4880 (16)	3.4803 (18)
Plane(4) –> Plane(3)[1545]	3.802 (2)	6.2(2)	3.4803 (18)	− 3.4880 (16)

[1545] = $x, -1+y, z$; [1565] = $x, 1+y, z$; [2666] = $1-x, 1-y, 1-z$; [2756] = $2-x, -y, 1-z$

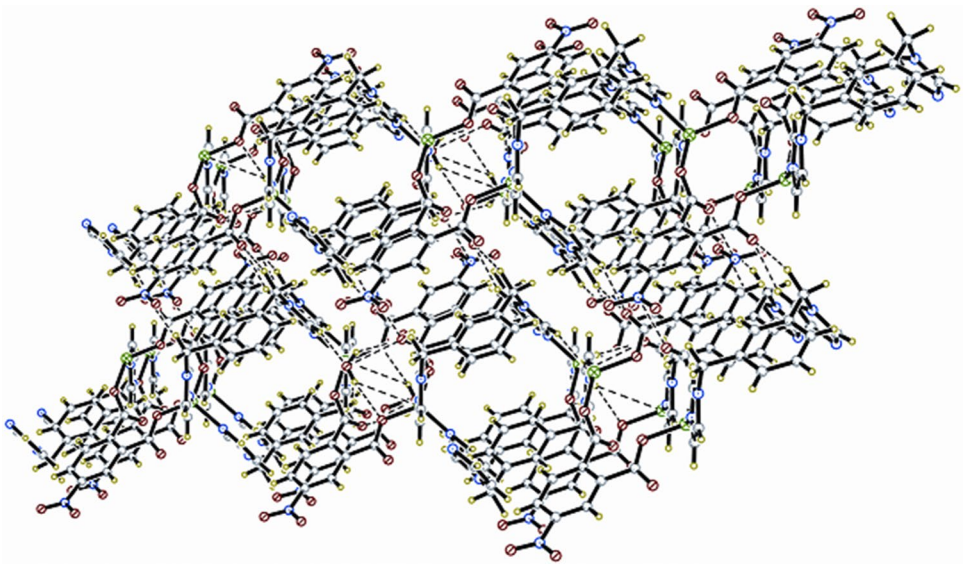

Fig. 6 View of the 3D supramolecular structure of **2** formed by hydrogen-bonding and π–π interactions

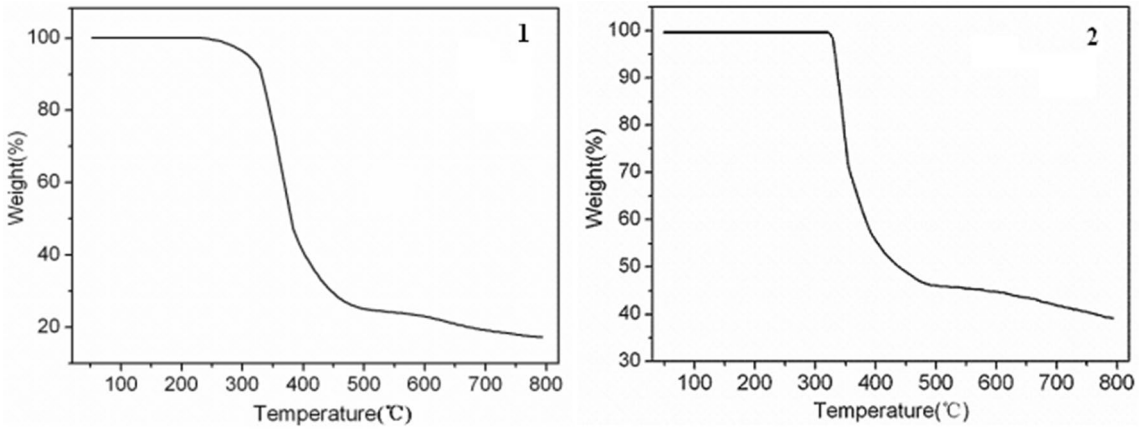

Fig. 7 TG curve of the complexes **1** and **2**

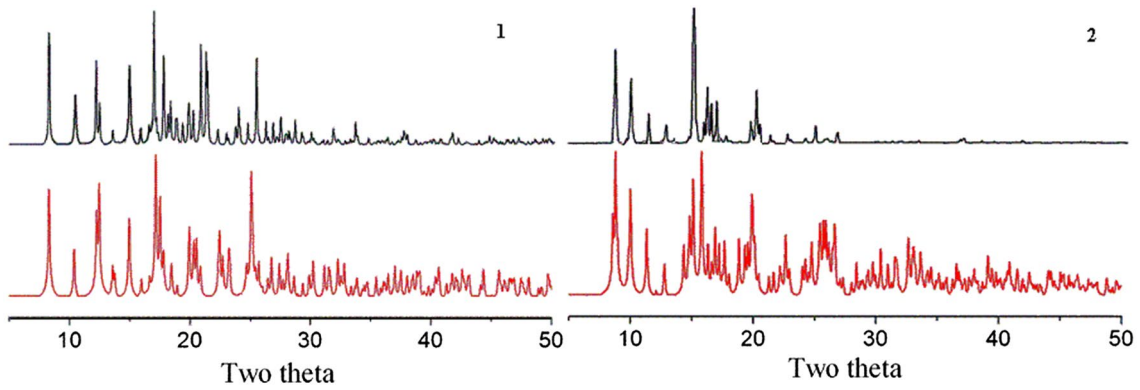

Fig. 8 PXRD analysis of complexes **1** and **2**: bottom-simulated, top-experimental

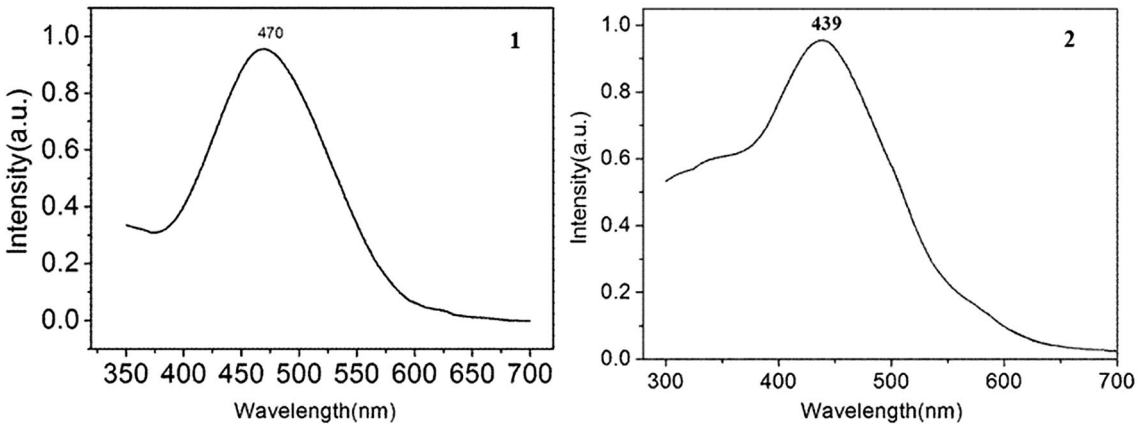

Fig. 9 Solid-state emission spectrum of **1** and **2** at room temperature

440 nm upon excitation at 280 nm, respectively. **1** shows strong emission band maxima approximately at 470 nm upon excitation at 292 nm. **2** exhibits the strong emission at 439 nm upon 270 nm excitation. It is obvious that the emission peaks of complex **1** is shift as compared to the free ligand 4-H_2nph/bix. Therefore, those emission bands of complex **1** may be assigned as ligand-to-metal charge transfer (LMCT) transitions [25]. While, because the d^{10} configuration Zn(II) is difficult to oxidize or reduce, the emissions are neither metal-to-ligand charge transfer (MLCT) nor LMCT. The emission bands of complex **2** could be assigned to the emission of ligand-to-ligand charge transfer [26–28].

3.5 Theoretical Calculations

All calculations in this work were carried out with the Gaussian03 program [29]. The parameters of the molecular structure for calculation were all from the experimental data of the complex. Natural bond orbital (NBO) analysis was performed by density functional theory (DFT) [30] with the PBE0 [31, 32] hybrid functional and the LANL2DZ basis set [33].

The selected natural atomic charges and natural electron configuration for the complex **1** is shown in Table 5. It is indicated that the electronic configurations of Ni(II) ion, N and O atoms are $4s^{0.28}3d^{8.29}4p^{0.47}$, $2s^{1.35}2p^{4.18}$ and $2s^{1.65\sim1.70}2p^{4.95\sim5.28}$, respectively. On account of the above results, one can infer that the Ni(1) ion coordination with

Table 5 Natural atomic charges, natural valence electron configurations, wiberg bond indexes and NBO bond orders(a.u) for **1** and **2**

Atom	Net charge	Electron configuration	Bond	Wiberg bond index	NBO bond order
1					
Ni(1)	0.96152	[core]4*s*(0.28)3*d*(8.29)4*p*(0.47)			
O(1)	−0.71871	[core]2*s*(1.65)2*p*(5.06)	Ni(1)–O(1)	0.3134	0.3399
O(3A)	−0.65830	[core]2*s*(1.68)2*p*(4.95)	Ni(1)–O(3A)	0.2140	0.2454
O(3B)	−0.65828	[core]2*s*(1.70)2*p*(5.02)	Ni(1)–O(3B)	0.2141	0.2456
O(6)	−0.95424	[core]2*s*(1.67)2*p*(5.28)	Ni(1)–O(6)	0.2079	0.2674
N(1)	−0.55214	[core]2*s*(1.35)2*p*(4.18)	Ni(1)–N(1)	0.2716	0.3550
N(1C)	−0.55154	[core]2*s*(1.35)2*p*(4.18)	Ni(1)–N(1C)	0.2713	0.3548
2					
Zn	1.33204	[core]4*s*(0.31)3*d*(9.97)4*p*(0.38)			
O(1)	−0.77255	[core]2*s*(1.70)2*p*(5.07)	Zn–O(1)	0.2788	0.3168
O(3A)	−0.82141	[core]2*s*(1.70)2*p*(5.11)	Zn–O(3A)	0.2907	0.3358
N(1)	−0.64245	[core]2*s*(1.41)2*p*(4.22)	Zn–N(1)	0.2328	0.3494
N(4B)	−0.68444	[core]2*s*(1.37)2*p*(4.30)	Zn–N(4B)	0.2049	0.3169

Symmetry codes: 1: (A) $x-1, y, z$; (B) $x-1, -y+1/2, z$; (C) $x, -y+1/2, z$

2: (A) $2-x, 1-y, 1-z$; (B) $2-x, 1-y, -z$

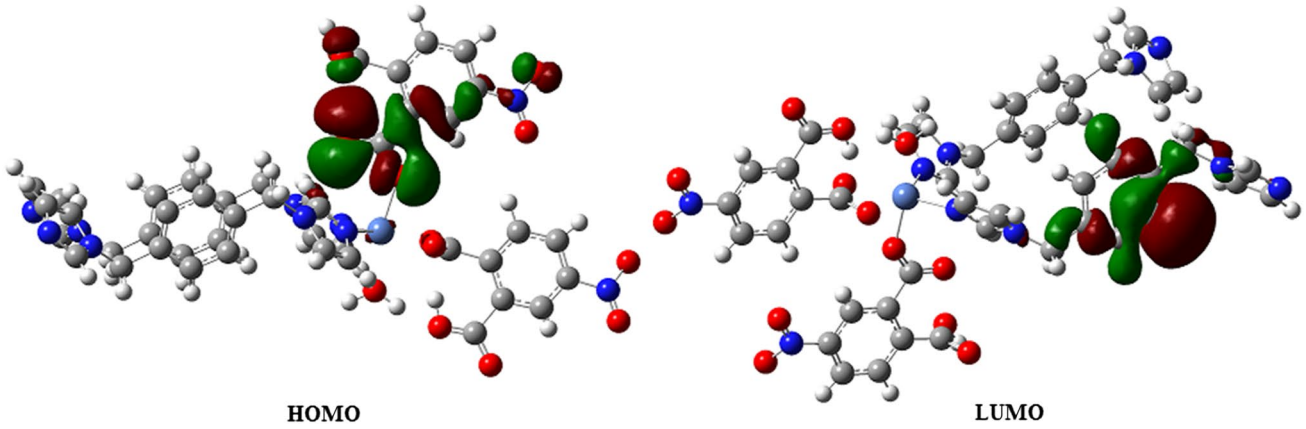

Fig. 10 Frontier molecular orbitals of complex **1**

N and O atoms is mainly on the 3*d*, 4*s* and 4*p* orbitals. N atoms form coordination bonds with Ni(1) ion using 2*s* and 2*p* orbitals. All O atoms provide electrons of 2*s* and 2*p* to the Ni(1) ion and form the coordination bonds.

Therefore, the Ni(II) ion obtained some electrons from two N atoms of bix ligands and four O atoms of 4-nph ligands [32, 33]. Thus, according to valence-bond theory, the atomic net charge distribution and NBO bond orders of **1** (Table 5) show obvious covalent interaction between the coordinated atoms and Ni(II) ion. The differences of NBO bond orders for Ni–O and Ni–N make their bond lengths different [34], which is in good agreement with the X-ray crystal structural data of complex **1**.

As can be seen from Fig. 10, the highest occupied molecular orbital (HOMO) is mainly composed of 4-nph ligands, whereas the lowest unoccupied molecular orbital (LUMO) mainly consists of bix ligands. Thereby, LLCT may be inferred from some contours of molecular orbital of complex **1**.

The selected natural atomic charges and natural electron configuration for the complex **2** is listed in Table 5. It is shown that the electronic configurations of Zn(II) ion, N and O atoms are $4s^{0.31}3d^{9.97}4p^{0.38}$, $2s^{1.37\sim1.41}2p^{4.22\sim4.30}$ and $2s^{1.70}2p^{5.07\sim5.11}$, respectively. In view of the above effects, one can infer that the Zn(II) ion coordination with N and O atoms is mainly on 3*d*, 4*s*, and 4*p* orbitals. N atoms form coordination bonds with Zn(II) ion using 2*s* and 2*p* orbitals. All O atoms provide electrons of 2*s* and 2*p* to Zn(II) ion and form the coordination bonds. So, the Zn(II) ion gained some electrons from two N atoms of mbix, two O atoms of 4-nph [32, 33]. Therefore, on the basis of valence-bond theory, the atomic net charge distribution and the NBO bond orders of the complex **2** (Table 5) shows the obvious covalent interaction between the coordinated atoms and Zn(II) ion. The differences of the NBO bond orders for Zn–O and Zn–N bonds make their bond

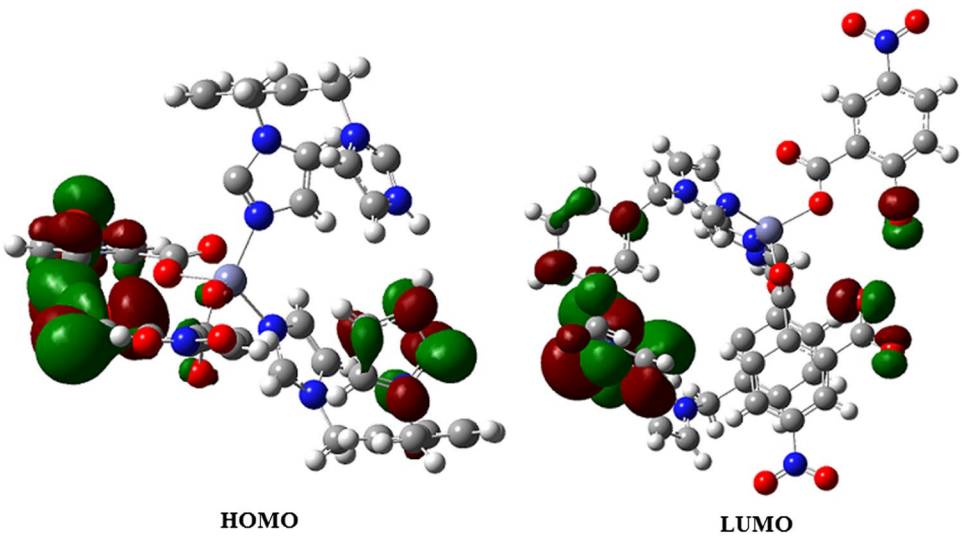

Fig. 11 Frontier molecular orbitals of complex **2**

lengths be different [34], which is in good agreement with the X-ray crystal structural data of complex **2**.

As shown in the Fig. 11, LUMO is mainly made up of mbix ligand, whereas highest occupied molecular orbital mainly composed of 4-nph ligand. So, LLCT be inferred from some contours of molecular orbital of complex **2**.

4 Conclusions

In summary, we have reported two new complexes formed by 4-nitrophthate and 1,4-bis(imidazol-1-yl)-benzene/1,3-bis(imidazol-1-yl)-benzene ligands. Complex **1** exhibits a two-dimensional (2D) network structure contain 42-number ring and complex **2** shows a one dimensional ribbon, which were further extended into a three-dimensional supramolecular structure through hydrogen bonds and π–π stacking interactions. Here we studied the synthesis, structure, TG and photoluminescent properties of the coordination polymers. This material will give new impetus to the construction of novel functional material with potentially useful physical properties. Moreover, we analyzed the NBO using the PBE0/LANL2DZ method in the Gaussian 03 program of complexes **1** and **2**. The calculation results indicated the obvious covalent interactions between the coordinated atoms and the Ni^{II}, Zn^{II} ion respectively.

Acknowledgements This work was supported by the Science and Technology Development Project of Jilin Provincial Science & Technology Department (Grant No. 2015052006JH) and the Science and Technology Research Projects of the Education Department of Jilin Province (Grant No. 2016219). Program supports from State Key Laboratory of Theoretical and Computational Chemistry of Tonghua Normal University are gratefully acknowledged.

References

1. Y.M. Zhang, S. Yuan, G. Day, X. Wang, X. Yang, H.C. Zhou, Coord. Chem. Rev. **354**, 28 (2018)
2. L. Mei, W.Q. Shi, Z.F. Chai, Bull. Chem. Soc. Jpn. **91**, 554 (2018)
3. R. Sakamoto, Bull. Chem. Soc. Jpn. **90**, 272 (2017)
4. L. Jiao, Y. Wang, H.L. Jiang, Q. Xu, Adv. Mater. **30**, 1703663 (2018)
5. J.S. Hu, L.F. Huang, X.Q. Yao, L. Qin, Y.Z. Li, Z.J. Guo, H.G. Zheng, Z.L. Xue, Inorg. Chem. **50**, 2404 (2011)
6. R. Cao, D.F. Sun, Y.C. Liang, M.C. Hong, K. Tatsumi, Q. Shi, Inorg. Chem. **41**, 2087 (2002)
7. P.M. Forster, A.R. Burbank, C. Livage, G. Férey, A.K. Cheetham, Chem. Commun. **33**, 368 (2004)
8. P. Mahata, S. Natarajan, Inorg. Chem. **46**, 1250 (2007)
9. B. Kesanli, Y. Cui, M.R. Smith, E.W. Bittner, B.C. Bockrath, W.B. Lin, Angew. Chem. Int. Ed. **44**, 72 (2005)
10. Q. Wu, M.J. Cao, B. Wei, Y. Bai, H. Tian, J. Wang, Q.Y. Liu, G.W. Yang, Inorg. Chem. Commun. **62**, 111 (2015)
11. Z.T. Wang, S.J. Wang, X.M. Li, Y.R. Pan, Chin. J. Struct. Chem. **37**, 467 (2018)
12. Z. Zhang, M. Pi, T. Wang, C.M. Jin, J. Mol. Struct. **992**, 111 (2011)
13. L. Croitor, D. Chisca, E.B. Coropceanu, G.F. Volodina, M.S. Fonari, J. Mol. Struct. **1137**, 136 (2017)
14. Z. Xing, Q.W. Wang, W. Sui, B. Liu, Chin. J. Struct. Chem. **37**, 125 (2018)
15. G.F. Li, Y.N. Wang, Q.W. Wang, X.M. Li, J.Y. Ji, Chin. J. Inorg. Chem. **30**, 2577 (2014)
16. X.M. Li, M. Sun, Y.R. Pan, J.Y. Ji, Chin. J. Struct. Chem. **35**, 298 (2016)
17. G.F. Li, Y.N. Wang, Q.W. Wang, X.M. Li, J.Y. Ji, Y.R. Pan, Chin. J. Inorg. Chem. **31**, 183 (2015)
18. X.M. Li, Z.T. Wang, Y.R. Pan, Q.W. Wang, B. Liu, J. Inorg. Organomet. Polym. Mater. **28**, 258 (2018)
19. G.M. Sheldrick, *SHELXS-97, Programs for X-ray Crystal Structure Solution* (University of Göttingen, Göttingen, 1997)
20. G.M. Sheldrick, *SHELXL-97, Programs for X-ray Crystal Structure Refinement* (University of Göttingen, Göttingen, 1997)
21. Y.R. Pan, M. Sun, X.M. Li, Chin. J. Struct. Chem. **34**, 710 (2015)
22. M. Devereux, D.O. Shea, A. Kellett, M. McCann, M. Walsh, D. Egan, C. Deegan, K. Kędziora, G. Rosair, H. Müller-Bunz, Inorg. Biochem. **101**, 881 (2007)
23. S. Ruchi, K.P. Bharadwaj, Cryst. Growth Des. **13**, 3722 (2013)
24. X. Bing, J. Xie, H.M. Hu, X.L. Yang, F.X. Dong, M.L. Yang, G.L. Xue, Cryst. Growth Des. **14**, 1629 (2014)
25. Y. Cui, Y. Yue, G. Qian, B. Chen, Chem. Rev. **112**, 1126 (2012)
26. G.G. Mohamed, N.E.A. El-Gamel, Spectrochim. Acta A **60**, 3141 (2004)
27. U. Mukhopadhyay, I. Bernal, Cryst. Growth Des. **5**, 1687 (2005)
28. G.L. Li, G.Z. Liu, L.L. Huang, L. Li, X. Zhang, J. Inorg. Organomet. Polym. **24**, 617 (2014)
29. M.J. Frisch, G.W. Trucks, H.B. Schlegel, G.E. Scuseria, M.A. Robb, J.R. Cheeseman, R.E. Stratmann, O. Yazyev, A.J. Austin, R. Cammi, C. Pomelli, J.W. Ochterski, P.Y. Ayala, K. Morokuma, G.A. Voth, P. Salvador, J.J. Dannenberg, V.G. Zakrzewski, S. Dapprich, A.D. Daniels, M.C. Strain, O. Farkas, D.K. Malick, A.D. Rabuck, K. Raghavachari, J.B. Foresman, J.V. Ortiz, Q. Cui, A.G. Baboul, S. Clifford, J. Cioslowski, B.B. Stefanov, G. Liu, A. Liashenko, P. Piskorz, I. Komaromi, R.L. Martin, D.J. Fox, T. Keith, M.A. AlLaham, C.Y. Peng, A. Nanayakkara, M. Challacombe, P.M.W. Gill, B. Johnson, W. Chen, M.W. Wong, C. Gonzalez, J.A. Pople, *Gaussian 03, Revision B.03* (Gaussian Inc, Pittsburgh, PA, 2003)
30. R.G. Parr, W. Yang, *Density Functional Theory of Atoms and Molecules* (Oxford University Press, Oxford, 1989)
31. C. Adamo, V.J. Barone, Chem. Phys. **110**, 6158 (1999)
32. M. Ernzerhof, G.E. Scuseria, J. Chem. Phys. **110**, 5029 (1999)
33. L. Wang, J. Zhao, L. Ni, J. Yao, J. Inorg. Gen. Chem. **638**, 224 (2012)
34. Z.P. Li, Y.H. Xing, Y.H. Zhang, Acta Phys. Chim. Sin. **25**, 741 (2009)